JOURNAL OF OCULAR PHARMACOLOGY AND THERAPEUTICS
Volume 23, Number 2, 2007

DOI: 10.1089/jop.2006.0118

Aloe-Emodin Metabolites Protected *N*-Methyl-D-Aspartate-Treated Retinal Ganglion Cells by Cu-Zn Superoxide Dismutase

HUI-JU LIN,[1–3] CHIEN-CHEN LAI,[2,4] PEI-DAWN LEE CHAO,[5] SENG-SHEEN FAN,[3] YUHSIN TSAI,[6] SHIUAN-YI HUANG,[2] LEI WAN,[2] and FUU-JEN TSAI[2,6]

ABSTRACT

A high concentration of glutamate in the eyes not only activates *N*-methyl-D-aspartate (NMDA) receptors, but also is toxic to the retina ganglion cells (RGCs) in glaucomatous patients. Our previous study had found that aloe-emodin sulfates/glucuronides metabolites, an anthraquinone polyphenol, exerted a neuroprotective activity upon RGCs. In order to understand the mechanisms involved in this neuroprotective effect, this study aimed to determine the expressions of RNAs and proteins in various treatments. The proteins expressed in the control group, NMDA-treated group, and aloe-emodin metabolites–cotreated group were separated by two-dimensional gel electrophoresis (2-DE). Protein spots were excised from 2-DE and analyzed by nano-LC-MS/MS (nano-liquid chromatography with mass spectrometry; tandem MS). Quantitative polymerase chain reaction (Q-PCR) was used to investigate the RNA related to these proteins. There were 84 spots with significant differences in various treatments. Among the 84 spots, we identified 9 spots whose functions were closely related to regulate the apoptosis of cells. The results of Q-PCR were not completely unanimous with those of 2-DE. Our results suggested that aloe-emodin metabolites decreased NMDA-induced apoptosis of RGCs by preserving, and inducing, some proteins related to the antioxidation and regulation of cells' energy. Both the level of RNA and protein of superoxide dismutase (Cu-Zn) were significantly elevated after aloe-emodin metabolites were added. The mechanisms of neuroprotection are complicated, and involve not only the transcription and stability of mRNA, but also post-translation protein modifications, degradation, and protein-protein interaction.

INTRODUCTION

GLAUCOMA IS A DISEASE characterized by a specific pattern of optic nerve head and visual field damage which, if not controlled, may lead to blindness.[1] Researchers tend to believe that glaucoma is a neurodegenerative disease, rather than just a disease of intraocluar pressure (IOP) being increased.[2,3] Therefore, there is an increasing interest in neuroprotective therapy that help for the pro-

[1]Department of Ophthalmology, China Medical University Hospital, Asia University, Taichung, Taiwan.
[2]Department of Medical Genetics, China Medical University Hospital, Taichung, Taiwan.
[3]Department of Life Science, Tunghai University, Taichung, Taiwan.
[4]Institute of Molecular Biology, National Chung Hsing University, Taichung, Taiwan.
[5]School of Pharmacy, China Medical University, Taichung, Taiwan.
[6]Graduate Institute of Chinese Medical Science, China Medical University, Taichung, Taiwan.

tection of nerve cells in the eye from damage occurring in glaucoma patients.[4,5] Indeed, there was evidence that neuroprotective treatments were beneficial to the damaged nervous system.[6,7–10]

Recent studies are consistent with the notion that excitotoxicity of glutamate is implicated in a variety of slowly progressing neurodegenerative disorders. In such diseases as Huntington's disease, Parkinson's disease, Alzheimer's disease, and multiple sclerosis, patients suffer moderately elevated glutamate concentrations for longer periods of time and trigger cellular processes in neurons, eventually leading to apoptotic-like cell death.[11,12] This type of slow, apoptotic-like excitotoxicity is also implicated in glaucoma.[13–15] Retinal ganglion cells (RGCs) can be damaged by glutamate released from dying RGCs.[6,9] The concentration of vitreous glutamate has been shown to be elevated in humans[16] and dogs[17] with primary glaucoma, as well as in monkeys with experimentally induced glaucoma.[16] These findings indicate that elevated glutamate levels and excitotoxicity play important roles in the pathologic change of RGCs in glaucoma.[18] There are several classes of glutamate receptors, but the loss of RGCs primarily resulted from glutamate binding to the *N*-methy-D-aspartate (NMDA) subtype.[13–15] Under the activated condition with glutamate, the NMDA receptor opens a channel that allows Ca^{+2} and other cations to move into the cells, which activates transcription factors to induce apoptosis of neuron cells.[19] In this study, we used NMDA-treated RGCs as an *in vitro* model to investigate glaucomatous neuropathy.

The pathogenesis of primary open-angle glaucoma (POAG) is not fully understood.[2] Changing concentration of nitric oxide, free radicals, neurotransmitters, and growth factors were all risk factors of promoting damage in nervous system.[20,21] Oxidative stress is one of these factors, which contributes to the etiologies of glaucoma and progression of optic neuropathy.[22] Antioxidant enzymes, such as superoxide dismutase (SOD), catalase, and glutathione peroxidase, have been isolated from aqueous humor.[23] Antioxidant supplementations have been proven to enhance the function of trabecular meshwork and protect the optic nerve.[24] Thus, antioxidants are potential candidates for neuroprotection in glaucomatous neuropathy.

Aloe-emodin is a plant polyphenol and a promising antioxidant.[25] Aloe-emodin scavenges oxygen-derived free radicals, interferes with free radical–producing systems, and increases the function of endogenous antioxidants.[26] Although several other bioactivities of aloe-emodin have been reported,[27,28] the parent compound aloe-emodin used for the *in vitro* model essentially could not be extrapolated to an *in vitro* effect because polyphenols were extensively metabolized into sulfates and glucuronides, even when administered intravenously (i.v.).[29–31] Therefore, aloe-emodin metabolites, mainly sulfates and glucuronides (s/g), prepared from the blood of rats administered aloe-emodin was used to mimic the real molecules derived from aloe-emodin, which circulate in the bloodstream. Our previous study showed that aloe-emodin metabolites significantly decreased the apoptosis of NMDA-treated RGCs (unpublished data).

Recently, there has been an intense interest in the study of global expressions of proteins, an approach known as expression proteomics. It is well established that for only a subset of the expression of mRNA significantly correlates with the abundance of the protein.[32,33] Moreover, post-translational modifications, including phosphorylation, glycosylation, and degradation, which are aberrantly regulated in many diseases, cannot be predicted by measuring the amount of mRNA or by studying nucleoside sequences. Therefore, proteomic studies are needed to overcome the limitations of the studies of mRNA. To investigate aberrant proteins' expression associated with NMDA-treated RGCs, we adopted a proteomic approach using two-dimensional gel electrophoresis (2-DE) to compare the proteins in the control group, the NMDA-treated group, and the aloe-emodin metabolites cotreated group. We identified a number of proteins' spots whose intensity differed between the groups. The proteins corresponding to these spots were identified by nano-LC-MS/MS (nano-liquid chromatography with mass spectrometry; tandem MS), and their expression in the level of RNA was also monitored. In this study, we investigated the mechanism of aloe-emodin metabolites as neuroprotectors in NMDA-treated RGCs by proteomic and quantitative polymerase chain reaction (Q-PCR) technology.

METHODS

Retinal ganglion cells (RGCs)

N18 cells, obtained from the Japanese Collection of Research Bioresources Bank, are rat RGCs AU1

that have been hybridized with neuroblastoma cells. The cells were placed into 75 cm^3 tissue culture flasks and grown at 37°C under a humidified 5% CO_2 and 95% air at one atmosphere in Dulbecco's modified Eagle's medium (DMEM; Merck Co.; Darmstadt, German), supplemented with 10% fetal bovine serum (FBS; Gibco BRL, Grand Island, NY), 1% penicillin-streptomycin (10 ng/mL of penicillin and 10 ng/mL of streptomycin) (Gibco BRL), each of the nonessential amino acids, vitamins, and 1% glutamine (Gibco BRL). The cells were at a density of 20×10^4 cells/flask at a final volume of 12 mL or on 6-well plates at a density of 3×10^4 cells/well at a final volume of 2 mL/well. Cells grown to approximate confluence were then incubated in a different condition. HAT (hypoxanthine–aminopterin–thymidine) medium (Sigma Chemical Co., St. Louis, MO) was used to select hybridomas among normal cell populations. The cells were cultured for several generations and checked for viability. N18 RGCs with a prominent dendritic process, and the cell viability, was checked after various concentrations of NMDA were added (Fig. 1A and 1B). To confirm the property of N18 cells, we stained the cells with anti-Thy-1 antibody, a specific marker for granulocytic linkage and neurons (data not shown). In order to define the N18 RGCs, N18 RGCs were stained with NMDA receptor NR1 antibodies (Sigma Chemical Co.) and some granulous particles were seen on the cells' body (Fig. 1C). The result was verified by comparing the negative control which fluorescein-isothiocyanate (FITC)-stained RGCs was not observed in N18 RGCs with the secondary antibody only. AMPA receptors (both GluR1 and GluR2), which were the other major glutamate receptors, were not observed in N18 RGCs. Moreover, the change of Ca^{2+} concentration was an important indicator of the NMDA receptor, and Mg^{2+} was incarcerated in the NMDA receptor channel. We checked the change of Ca^{2+} concentration with and without Mg^{2+} by flow cytometry. The result revealed that an intracellular Ca^{2+} concentration of N18 RGCs was increase in the Mg^{2+}-free medium (data not shown). This also proved that N18 RGCs were suitable for NMDA-receptor studies.

Our previous study had revealed that NMDA at 100 μM accounted for 69.9% of the apoptosis of N18 RGCs, and that 15 μM of aloe-emodin metabolites was able to decrease the NMDA-induced apoptosis of RGCs from 69.9% ± 2.1% to

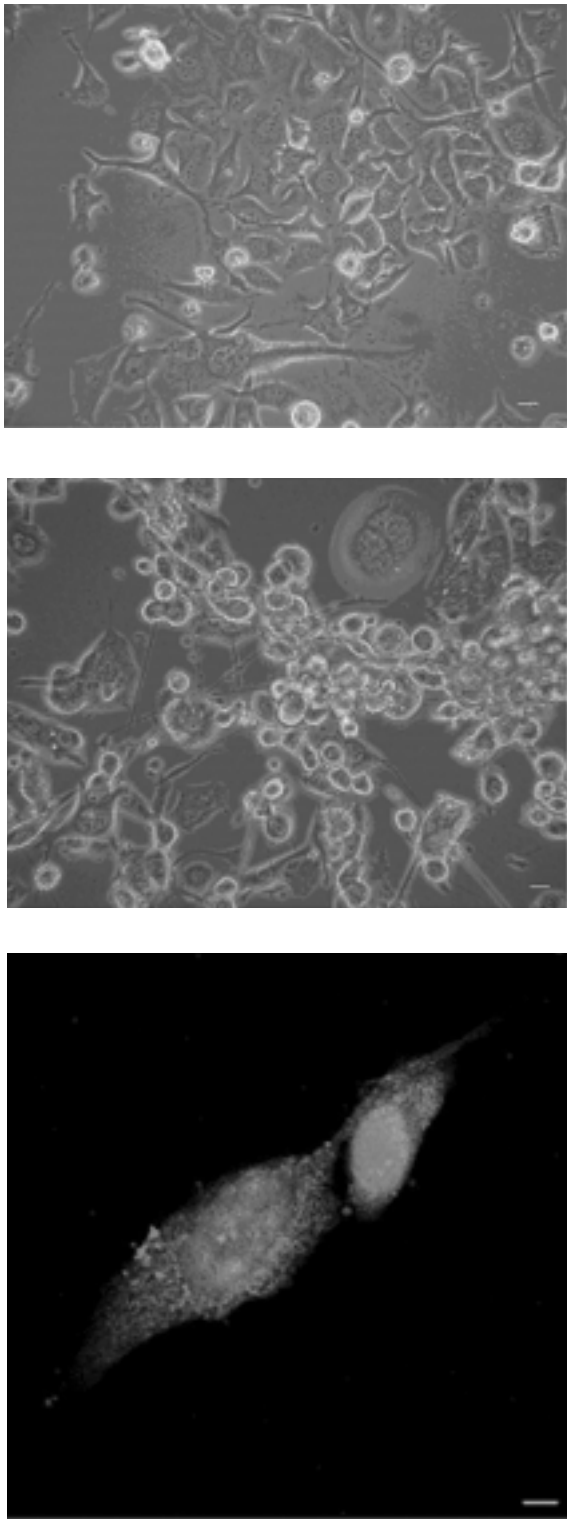

FIG. 1. **(A)** Some retinal ganglion cells (RGCs) died after 100 μM *N*-methyl-D-aspartate (NMDA) was added; the dead RGCs floated up (scale bar = 1 μm); **(B)** Some RGCs died after 5 mM NMDA was added; the dead RGCs floated up. The RGCs were more prone to death then when in 100 μM NMDA. (Scale bar 1 = μm). **(C)** RGCs stained with anti-NR1 antibody labeled with fluorescein-isothiocyanate (FITC; scale bar = 0.3 μm).

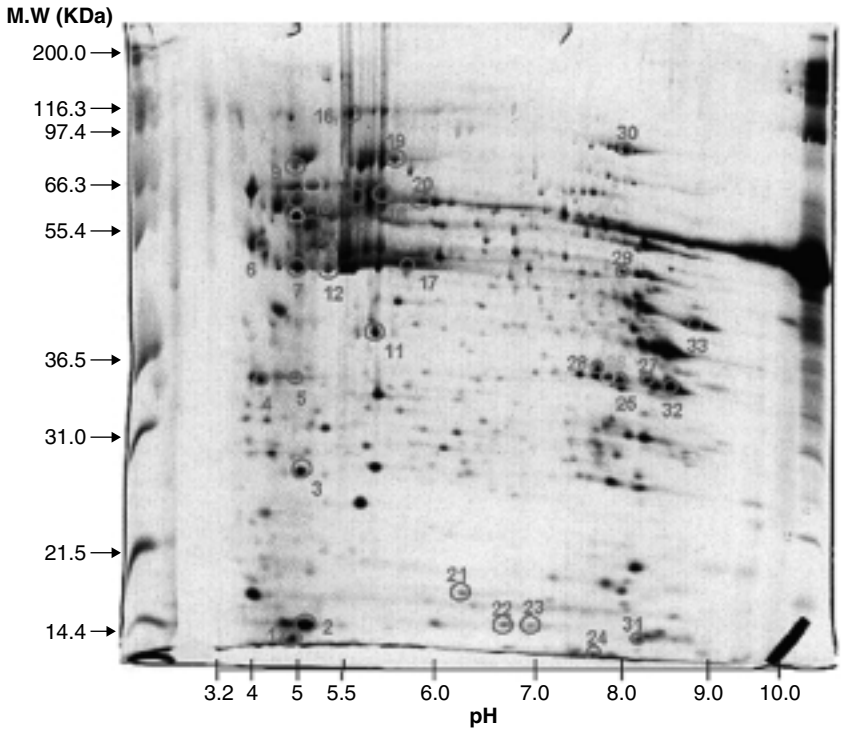

FIG. 2. Spots 1–33 appeared only when aloe-emodin was added to the cells and did not appear in the negative control or when *N*-methyl-D-aspartate only was added to the cells.

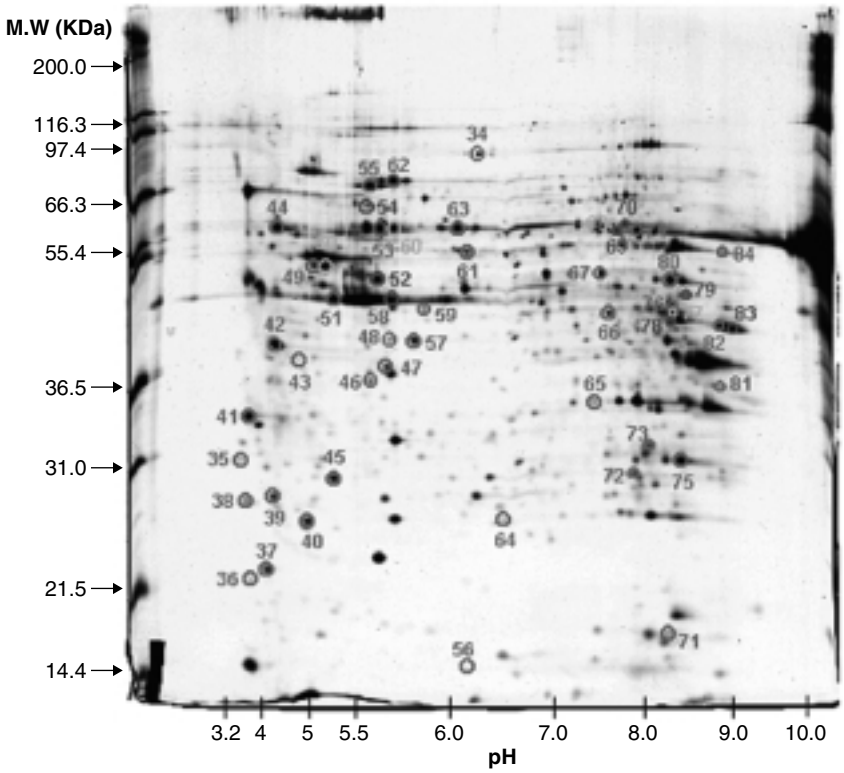

FIG. 3. Spots 34–84 appeared in the negative control and after aloe-emodin was added to the *N*-methyl-D-aspartate (NMDA)-treated cells but did not exist in the cells treated with NMDA only.

50% ± 2.5% (data not shown; unpublished data). To correct for variability, quartet gels were run for each experimental condition. Proteins were considered to be significantly upregulated when the corresponding spot volumes showed an increase by a factor of at least two. Representative master 2-DE gels as shown in Figures 2 and 3, displayed proteins that were preserved or expressed after cotreated RGCs with aloe-emodin metabolites and NMDA. The proteins varied from 10 to 120 kDa in size, with pI values ranging from 3 to 10.

F2,3

AU2

Preparation and quantification of aloe-emodin metabolites from rats: Chemicals

Aloe-emodin and PEG 400 were purchased from Sigma Chemical Co. LC-grade acetonitrile, ethyl acetate, and methyl alcohol were obtained from Mallinckrodt Baker, Inc. (Phillipsburg, NJ). Milli-Q plus Water (Millipore; Bedford, MA) was used for all preparations.

Animal protocol and drug administration for preparing aloe-emodin metabolites

Male Sprague-Dawley rats, weighing 250∼300 g, were fasted for 12 h before the drug administration. Aloe-emodin was dissolved in PEG 400 and administered to rats. Blood was withdrawn by cardiac puncture at 5 min after dosing, and the serum was obtained after centrifugation at 9860*g* for 15 min. The animal study adhered to the ARVO Statement for the Use of Animals in Ophthalmic and Vision Research.

Quantification of aloe-emodin metabolites in serum

Serum was vortexed with a fourfold volume of methanol, then centrifuged at 9860*g* for 15 min to remove the precipitate. The supernatant was evaporated under a vacuum. The residue was then dissolved in water and purified through solid-phase extraction, using Strata (Phenomenex). The concentrations of glucuronides and sulfates of aloe-emodin (aloe-emodin s/g) were determined by high-performance liquid chromatography (HPLC) after hydrolysis with β-glucuronidase and sulfatase, respectively.

AU3

2-DE and image analysis

An aliquot containing 100 μg of protein sample was diluted with 350 μL of rehydration buffer containing 8 M of urea, 4% CHAPS, 65 mM of dithioerythreitol (DTE), 0.5% ampholytes, and a trace of bromophenol blue. The sample was hydrated of a 17-cm strip and immobilized to a pH gradient of 3–10 (ReadyStrip IPG strip; Bio-Rad) overnight; the sample was focused for a total of 60 kVh (PROTEAN IEF cell; Bio-Rad) at 20°C and then stored at −80°C. Strips were equilibrated with 3 mL of an equilibrium solution containing 50 mM of Tris-HCl (pH 8.8), 6 M of urea, 30% glycerol, 2% sodium dodecyl sulfate (SDS), a trace of bromophenol blue, and DTE (1% w/v) for 20 min, followed by equilibration for 20 min in the same solution, containing iodoacetamide (2.5% w/v) instead of DTE. The strips were transferred to the top of 12% polyacrylamide gels and held in position with molten 0.5% agarose in running buffer containing 25 mM of Tris, 0.192 M of glycine, and 0.1% SDS. Gels were run at 16 mA for 30 min, followed by 50 mA for 4∼5 h. Gels were routinely stained with silver nitrate and then scanned by a GS-800 imaging densitometer, with PDQuest software, version 7.1.1 (Bio-Rad). To evaluate intrasample and intersample variability, gels were analyzed in the following manner: Protein spots from each gel were detected and matched automatically; a master gel image was generated from the matched gel sets; and finally, the intensity of the spots was compared among gels. Data were exported to Microsoft Excel for the creation of the correction- and spot-intensity graphs.

AU4

AU5

In-gel protein digestion

A slightly modified procedure, originally developed by Terry and colleagues, was used for the in-gel digestion of proteins from silver-stained gels for nano-LC-MS/MS.[34] Briefly, each spot of interest in the silver-stained gel was sliced into 1-mm cubes. The proteins in these gels were reduced and methylated with 50 mM of DTE and 100 mM of iodoacetamide (IAA) in 50 mM of ammonium bicarbonate. These gel pieces were washed two times with 50% v/v acetonitrile (ACN) in 100 mM of ammonium bicarbonate buffer (pH 8.0) for 10 min at room temperature. They were then soaked in 100% ACN for 5 min, dried in a lyophilizer for 20–30 min, and rehydrated in 50 mM of ammonium bicarbonate buffer (pH 8.0) containing 10 μg/mL of trypsin (Promega; Madison, WI) until the gel pieces were fully immersed. After incubating for 16–20 h at

30°C, the remaining trypsin solution was transferred into a new microtube. The gel pieces were resuspended with 50% ACN in 5.0% formic acid (FA) for 60 min and then concentrated to dryness.

Nanoelectrospray mass spectrometry

Nanoscale capillary LC-MS/MS was used to analyze the meaningful proteins involved in the reaction. LC-MS/MS analysis was performed using an Ultimate capillary LC system (LC Packings; Amsterdam, The Netherlands) coupled to a QSTARXL quadrupole-time of flight (Q-TOF) mass spectrometer (Applied Biosystem/MDS Sciex; Foster City, CA). The nanoscale capillary LC separation was performed on a RP C18 column (15 × 75 cm i.d.), with a flow rate of 200 nL/min and a 60-min linear gradient of 5%–50% of buffer B. Buffer A contained 0.1% FA in 5% aqueous ACN; buffer B contained 0.1% FA in 95% aqueous ACN. The nanoLC tip for online LC-MS was a PicoTip (FS360-20-10-D-20; New Objective, Cambridge, MA). Data were acquired by automatic Information Dependent Acquisition (IDA; Applied Biosystem/MDS Sciex). The IDA automatically finds the most intense ions in a TOF MS spectrum, and then performs an optimized MS/MS analysis on the selected ions. The product ion spectra generated by nanoLC-MS/MS were searched against NCBI databases for exact matches, using the ProID program (Applied Biosystem/MDS Sciex) and the MASCOT search program (www.matrixscience.com).[35] A mammalian taxonomy restriction was used, and the mass tolerance of both precursor ion and fragment ions was set to ±0.3 Da. Carbamidomethyl cysteine was set as a fixed modification, whereas serine, threonine, tyrosine phosphorylation, and other modifications were set as variable modifications. All identified phosphopeptides were confirmed by manual interpretation of the spectra.

RNA isolation

RNA was extracted from RGCs, using 250 μL of TRIZOL reagent, according the manufacturer's instructions (Biotecx; Friendswood, TX). The protocol included cell lysis, extraction of the organic fraction with chloroform, and precipitation of RNA with isopropanol. RNA concentrations were calculated at an absorbance from the absorbance at 260 nm. An aliquot containing 0.2 μg of total RNA was mixed with dNTP (20 μM), 3′primer (0.25 μM), and reverse-transcription (RT) buffer (1×, BRL) in a total volume of 19 μL and was heated at 65°C for 5 min and then at 37°C for 10 min; 1 μL of MMLV RT (200 μL) was then added and incubated at 37°C for 50 min, followed by 95°C for 5 min, to inactivate the reverse transcriptase. At the end of the transcription, the tubes were either placed on ice for polymerase chain reaction (PCR) or stored at −20°C for later use.

Quantitative polymerase chain reaction (Q-PCR)

Q-PCR was used to investigate the quantity of RNA in the reaction. Total RNA was extracted with TRIZOL reagent (Invitrogen), according to the manufacturer's protocol. For each cDNA sample, a ratio of the relative amounts of target gene and GAPDH was calculated to compensate for variations in the quantity or quality of starting mRNA, as well as for the differences in RT efficiency. The fold change in the target gene relative to the GAPDH endogenous control gene specific to forward and reverse primers were designed using the LightCycler Probe Design software (Roche Applied Science), based on sequence data from the hemerythrin nucleic acid sequence. The primer sequences and reactive conditions were listed in the Table 1. The fold change in the target gene relative to the GAPDH endogenous control gene was calculated according to a method previously proposed,[36] fold change = 2□(□CT), where □CT = CT, target − CT, GAPDH and □(□CT) = □CT, treated − □CT, control. RT-PCRs were run separately for each candidate in triplicate, and data were analyzed for statistical differences by the Mann–Whitney U test, using PRISM 4.0 software (GraphPad; San Diego, CA).

AU6 AU7 T1 AU8 AU8

RESULTS

Various concentrations of NMDA were tested and 100 μM was able to induce 69.9% of apoptosis in RGCs, which was suitable for evaluating drug efficacy. Besides, 15 μM of aloe-emodin metabolites was able to decrease NMDA-induced apoptosis of RGCs from 69.9% ± 2.1% to 50% ± 2.5% (data not shown; unpublished data).

Table 1. Primers and Conditions for Quantitative Polymerase Chain Reaction

GAPDH	5′-AGCTTGTCATCAACGGGAAG-3′ 5′-TTTGATGTTAGTGGGGTCTCG-3′ 95° C for 10 min 40 cycles; 95°C for 15 s, 59°C for 60 sec
Galectin-1	F: 5′-CTTCGCTTCATCATCATGGCCT-3′ R: 5′-AATGGTGTTGGCATCTCGT-3′ 95° C for 10 min 40 cycles; 95°C for 15 s, 59°C for 60 sec
EF 1-β	F: 5′-TGATAAGGTTGGAACAGATTTGC-3′ R: 5′-GACTGTACGTAGTCCTCAAAAGCA-3′ 95° C for 10 min 40 cycles; 95°C for 15 s, 59°C for 60 sec
Hsp60	F: 5′-AGGAAAAGCTGAACGAGCGA-3′ R: 5′-ATGAATCCAAGGCTGGGATG-3′ 95° C for 10 min 40 cycles; 95°C for 15 s, 59°C for 60 sec
Stress-70	F: 5′-GGTAAGATTTTCACCCCTGAAG-3′ R: 5′-TGTAAAACCTTAAATGGGTATCTGC-3′ 95° C for 10 min 40 cycles; 95°C for 15 s, 59°C for 60 sec
Cu-Zn SOD	F: 5′-CATTCCCTATGTGGTCTGAGTCT-3′ R: 5′-CAGTTTAATGGTTTGGTTTCTACAGT-3′ 95° C for 10 min 40 cycles; 95°C for 15 s, 59°C for 60 sec
Hsp10	F: 5′-GAGGGGCTTGTTCTTTCACC-3′ R: 5′-AAGGGGAGCACTTTCTAGGC-3′ 95° C for 10 min 40 cycles; 95°C for 15 s, 60°C for 60 sec
VDAC-1	F: 5′-GGATTTGGTTTTGGGTTGGT-3′ R: 5′-TTCCACACCACTGCATGACT-3′ 95° C for 10 min 40 cycles; 95°C for 15 s, 59°C for 60 sec
Mitofilin	F: 5′-TAGCGCAACAGAAAGCCACA-3′ R: 5′-TCCGCATTTCATTCTCCATG-3′ 95° C for 10 min 40 cycles; 95°C for 15 s, 59°C for 60 sec
PDI A6 precursor	F: 5′-AGGTGAAATTGGCAGCCGTA-3′ R: 5′-CCCTTGACACTATGTCAGATCTCGT-3′ 95° C for 10 min 40 cycles; 95°C for 15 s, 59°C for 60 sec

EF-1β, elongation factor 1-beta; Hsp 60, 60 kDa heat shock protein; Cu-Zn SOD, superoxide dismutase [Cu-Zn]; Hsp 10, 10 kDa heat shock protein; VDAC-1, voltage-dependent anion-selective channel protein 1; mitofilin, mitochondrial inner-membrane protein; PDI, protein disulfide-isomerase; A6, precursor

Changes in protein composition of control, NMDA, and aloe-emodin metabolites cotreated RGCs

Thirty-three (33) spots were selected at first, but they were only in the aloe-emodin metabolites and NMDA cotreated group, and were absent in the negative control or only the NMDA-added group (the expression of the 33 proteins were induced by the aloe-emodin metabolites; Fig. 2). Furthermore, 51 spots were expressed both in the control and in the aloe-emodin metabolites-treated group, but were not expressed in the NMDA-treated group (the expressions of the 51 proteins were preserved from their original condition; even NMDA and aloe-emodin metabolites were added to the N18 RGCs; Fig. 3). In gel digestion and nano-LC-MS/MS, analyses were processed for gel pieces from 84 spots labeled in Figures 2 and 3. The identification of 84 protein spots were listed in Table 2. All identifications were manually validated by taking into account the MOWSE score, apparent versus predicted isoelectric points, and the molecular weights, as well as the error distribution of apparent versus predicted peptide masses (m/z).

Identification of neuroprotection-related proteins

The focus of this study was placed on the proteins involved in the defense of oxidation, stress, and apoptosis. The selective criterion of the proteins was that the expression of proteins had to be twofold over the differential expressions. The distributions of involved proteins were as follows and are listed in Figure 4: stress-evoked proteins, 7.8%; proteins involved in cell growth, 6.3%; housekeeping proteins, 23.4%; proteins involved in the production of energy in cells, 31.3%; proteins involved in the formation of cell structures, 14.1%; and miscellaneous proteins, 17.2%. Among the 84 spots, we identified 9 proteins for further study. There were 2 stress-evoked proteins, 2 proteins involved in cell

TABLE 2. PROTEINS IDENTIFIED FROM MASS SPECTROMETRY

Spot no.	*Accession no.*	*Protein identification*	*MW (Kda) /pI*	*Score*	*Post-translational modification*
1		Beta-lactoglobulin	18.3/4.8	64	
2	PI6045	Galectin-1	14.7/5.3	146	
3	P70296	Phosphatidylethanolamine-binding protein	20.7/5.2	76	
4	O70251	Elongation factor 1-beta	24.5/4.5	42	
7		Beta-acin	39.1/5.8	75	
8	P02554	Tubulin beta chain	49.8/4.8	67	
11		Pyruvate dehydrongenase (lipoamide) beta	38.9/6.4	256	
12	P62739	Alpha-actin 2	42.0/5.2	48	
13	P56480	ATP synthase beta chain	56.3/5.2	588	
14		Calreticulin	48.0/4.3	130	
15	P63038	60 kDa heat shock protein	60.9/5.9	759	Oxidation (M55, M256, M477)
16		Tumor rejection antigen gp96	92.4/4.7	307	
17		Beta-actin	39.2/5.8	266	Oxidation (M299)
18	P63038	60 kDa heat shock protein	60.9/5.9	585	
19	P38647	Stress-70 protein	73.5/5.9	580	Deamidation (268)
20	P27773	Protein disulfide-isomerase A3	56.6/6.0	426	
21	P08228	Superoxide dismutase [Cu-Zn]	15.8/6.0	169	
22	P70349	Histidine triad nucleotide-binding protein 1	13.6/6.4	70	
24	Q64433	10 kDa heat shock protein	10.8/8.2	70	
27	P00348	Short chain 3-hydroxyacyl-CoA dehydrogenase	34.1/9.0	63	
28	Q60930	Voltage-dependent anion-selective channel protein 2	31.7/7.4	245	
30		Aconitase 2	85.4/8.1	990	Oxidation (m34, M393) Deamidatiaon (N626)
31	P62962	Profilin I	14.8/8.5	150	Deamidation (N61)
32	Q60932	Voltage-dependent anion-selective channel protein 1	32.3/8.6	373	Deamidation (N252)
33	P05202	Aspartate aminotransferase (Transaminase A)	47.4/9.1	261	Deamidation (N322)
34	Q8CAQ8	Mitochondrial inner-membrane protein (Mitofilin)	83.8/6.2	377	
35	Q9QZ23	HIRA-interacting protein 5	22.1/4.2	91	
38	P70580	Membrane associated progesterone receptor component 1	21.5/45.5	57	
39	P63028	Translationally controlled tumor protein	19.5/4.8	120	
40	P70296	Phosphatidylethanolamine-binding protein	20.7/5.2	138	
41	O35658	Complement component 1, Q subcomponent binding protein	31.0/4.8	79	
42	Q61937	Nucleophosmin	32.5/4.6	313	
44	P09103	Protein disulfide-isomerase precursor	57.1/4.8	780	Oxidation (M26, M358, M427)
45	Q9R0P9	Ubiquitin carboxyl-terminal hydrolase isozyme L1	24.8/5.1	119	
46	P11177	Pyruvate dehydrogenase E1 component beta subunit	39.2/6.2	74	
47		G protein beta 1 subunit	37.4/5.5	308	
49	Q63081	Protein disulfide-isomerase A6 precursor	47.2/5.0	144	
50	P52597	Heterogeneous nuclear ribonucleoprotein F	45.5/5.4	155	
51		Beta-actin	39.1/5.8	99	

(*continued*)

Table 2. Proteins Identified from Mass Spectrometry (Cont'd)

Spot no.	*Accession no.*	*Protein identification*	*MW (Kda) /pI*	*Score*	*Post-translational modification*
52	Q9CZ13	Ubiquinol-cytochrome-c reductase complex core protein I	52.7/5.8	414	Deamidation (86) Oxidation (M229, M440, M475)
53	P63038	60 kDa heat shock protein	60.9/5.9	770	Oxidation (M55, M40, M146, M217, M230, M316, M356, M13, M506) Deamidation (N136, Q496)
54	p63038	60 kDa heat shock protein	60.9/6.0	156	
55		Hsc70-ps1	70.9/5.4	516	Oxidation (m61, M549) Deamidation (N57, N355)
57	P50213	Isocitrate dehydrogenase [NAD] subunit alpha	39.6/6.5	181	
58	P18242	Cathepsin D precursor	44.9/6.7	88	
59		Hypothetical protein 4732456N10	58.2/8.5	75	Deamidation (N307)
60	P15331	Peripherin	54.2/5.4	490	Oxidation (M863, M391)
61	P31943	Heterogeneous nuclear ribonucleoprotein H	49.1/5.9	74	
62	P38647	Stress-70 protein	73.5/5.9	662	Deamidation (N149, N188) Oxidation (M172)
63	P27773	Protein disulfide-isomerase A3	56.6/6.0	505	Phospho (Y67, H126, S149, H167, Y478) Deamidation (N212, N473) Oxidation (M337, M433)
65	P68002	Voltage-dependent anion-selective channel protein 2	31.6/7.5	86	
66	Q15365	Poly(rC)-binding protein 1	37.5/6.7	114	
67	P18242	Cathepsin D	44.9/6.7	119	
71	P14851	Peptidyl-prolyl cis-trans isomerase A	17.8/8.5	37	
72	P02662	Alpha-S1 casein precursor	24.5/5.0	50	
74	Q9D0K2	Succinyl-CoA:3-ketoacid-coenzyme A transerase 1	56/8.3	18	Oxidation (M1110 Deamidation (N482)
75	Q9DCW4	Electron transfer flavoprotein beta-subunit	27.3/8.6	162	
77	Q8QZT1	Acetyl-CoA acetyltransferase	44.8/8.7	179	
78	P04075	Fructose-bisphophaate aldolase A	39.3/8.4	63	
79	Q04467	Isocitrate dehydrogenase	50.8/9.0	35	
80	P97807	Fumarate hydratase	54.3/9.1	190	
81		Heterogeneous nuclear ribonucleoprotein A2/B1 isoform 1	36.0/8.7	130	Oxidation (M41)
82	P05202	Aspartate aminotransferase	47.4/9.1	162	Oxidation (M281)
83	P05202	Aspartate aminotransferase	47.4/9.1	180	Deamidation (N322)
84	P19483	ATP synthase alpha chain heart isoform	59.7/9.2	170	

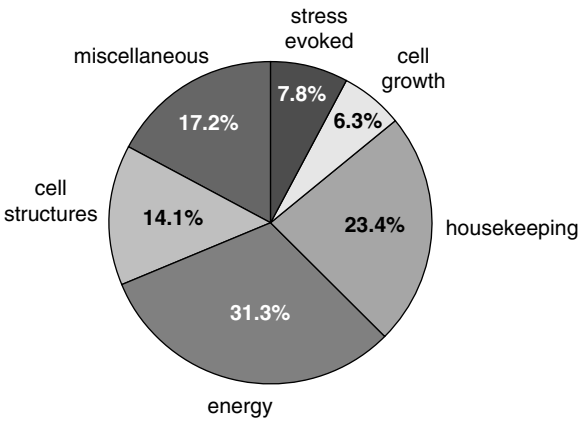

FIG. 4. The distributions of involved proteins: **(A)** Stress-evoked proteins; **(B)** proteins involved in cell growth; **(C)** housekeeping proteins; **(D)** proteins involved in the production of energy in cells; **(E)** proteins involved in the formation of cells structure; and **(F)** miscellaneous proteins.

growth, 3 proteins involved in the production of energy, and 2 proteins related to the formation of cells' structures (Table 3). Based on nano-LC-MS/MS, these spots (spots 2, 4, 15, 19, 21, 24, 32, 34, and 44; Fig. 5) were identified. Their nano-LC-MS/MS spectra are shown in Figure 5A–I, respectively. Tryptic peptides from these spots matched those predicted for these proteins. Their positions on the 2-DE gel are in agreement with the theoretical pIs and MWs, respectively. The proteins were characterized as galectin-1, elongation factor 1-beta (EF 1-β), 60 kDa heat shock protein (Hsp 60), stress-70 protein, superoxide dismutase [Cu-Zn] (Cu-Zn SOD), 10 kDa heat shock protein (Hsp 10), voltage-dependent anion-selective channel protein 1 (VDAC-1), mitochondrial inner membrane protein (mitofilin), and protein disulfide-isomerase (PDI) A6 precursor. Of these proteins, galectin-1, EF 1-β, Hsp 60, stress-70 protein, Cu-Zn SOD, Hsp 10, and VDAC-1 were prominently expressed only when aloe-emodin metabolites were added to the N18 RGCs and were not expressed in the control group, indicating that these proteins were induced by aloe-emodin metabolites. Mitofilin and the PDI A6 precursor were expressed significantly both in the control and aloe-emodin metabolites cotreated with N18 RGCs. This meant that mitofilin and the PDI A6 precursor were naturally expressed in N18 RGCs and acted as elements in the function of neuroprotection.

Table 3. Important Proteins Identified from Mass Spectrometry and the Results of Quantitative Polymerase Chain Reaction

Spot no.	*Protein identification*	*Functional classification*
2	Galectin-1	This protein binds beta-galactosidase. Its physiological function is not yet known. It may act as an autocrine negative growth factor that regulates cell proliferation.
4	Elongation factor 1-beta	EF-1-beta and EF-1-delta stimulate the exchange of GDP bound to EF-1 alpha to GTP. Phosphorylation affects the GDP/GTP exchange rate.
15	60 kDa heat shock protein	Implicated in mitochondrial protein import and macromolecular assembly. It interacts with p21Ras
19	Stress-70 protein	Implicated in the control of cell proliferation and cellular aging. May also act as a chaperone.
21	Superoxide dismutase [Cu-Zn]	Destroys radicals which are normally produced within the cells and which are toxic to biological systems 2 superoxide + 2 H^+ = O_2 + H_2O_2
24	10 kDa heat shock protein	Eukaryotic CPN10 homolog which is essential for mitochondrial protein biogenesis, together with CPN60. Binds to CPN60 in the presence of Mg-ATP and suppresses the ATPase activity
32	Voltage-dependent anion-selective channel protein 1	Forms a channel through the mitochondrial outer membrane and also the plasma membrane
34	Mitochondrial inner membrane protein (mitofilin)	Mitochondrial inner membrane protein
44	Protein disulfide-isomerase A6 precursor	Catalyzes the rearrangement of —S—S bonds in proteins

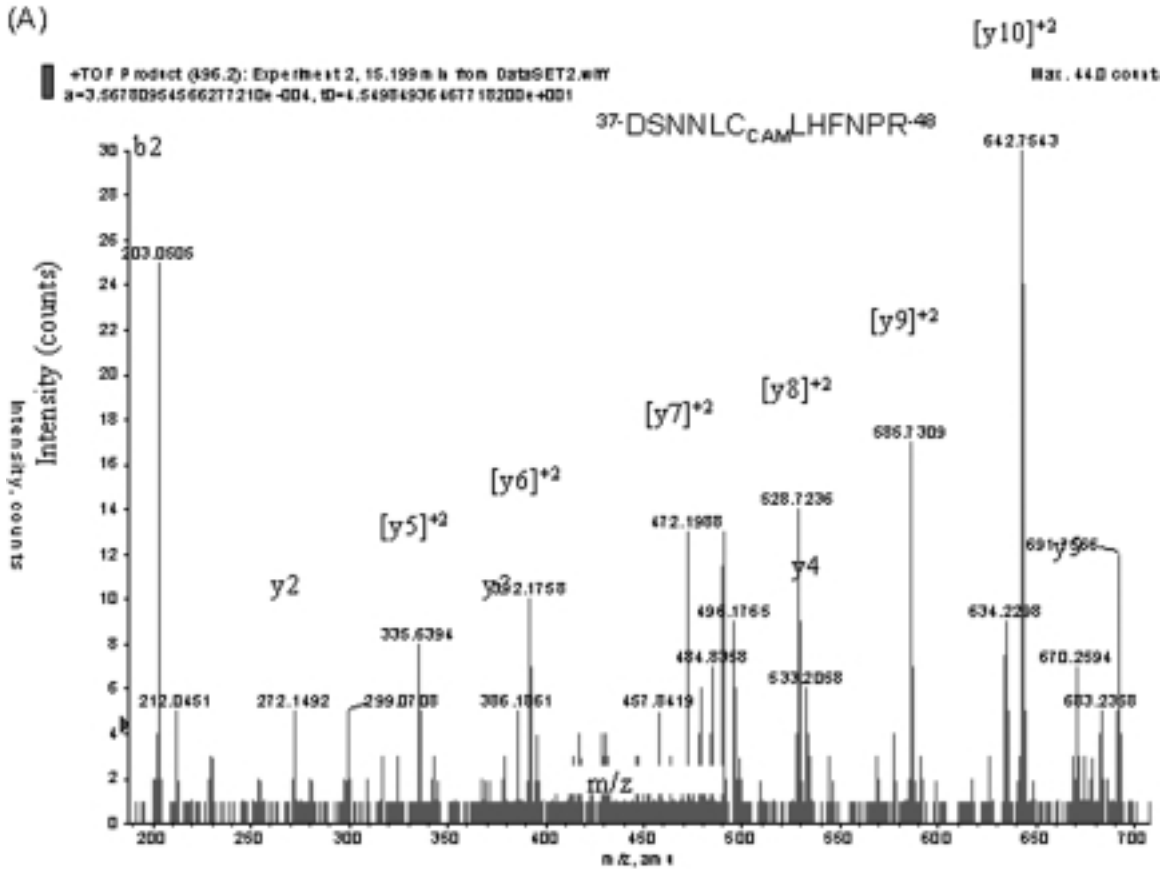

FIG. 5. Identification of galectin-1, EF 1-β, Hsp60, stress-70 protein, Cu-Zn SOD, Hsp10, VDAC-1, mitofilin, and PDI A6 precursor. **(A)** The nanoelectrospray mass spectrum of the triply charged ion m/z 496.22 for spot 2 is shown. The amino acid sequence, DSNNLCLHFNPR, was determined from mass differences in the y-fragment ion series and matched residues 37–48 of the mouse galectin-1. **(B)** The nanoelectrospray mass spectrum of the doubly charged ion m/z 809.42 for spot 4 is shown. The amino acid sequence, TPAGLQVLNDYLADK, was determined from mass differences in the y-fragment ion series and matched residues 7–21 of the mouse EF 1-β. **(C)** The nanoelectrospray mass spectrum of the doubly charged ion m/z 752.87 for spot 15 is shown. The amino acid sequence, TLNDELEIIEGMK, was determined from mass differences in the y-fragment ion series and matched residues 206–218 of the mouseHsp60. **(D)** The nanoelectrospray mass spectrum of the doubly charged ion m/z 725.83 for spot 19 is shown. The amino acid sequence, TTPSVVAFTADGER, was determined from mass differences in the y-fragment ion series and matched residues 86–99 of the stress-70 protein. **(E)** The nanoelectrospray mass spectrum of the doubly charged ion m/z 587.76 for spot 21 is shown. The amino acid sequence, DGVANVSIEDR, was determined from mass differences in the y-fragment ion series and matched residues 92–102 of the Cu-Zn SOD. **(F)** The nanoelectrospray mass spectrum of the doubly charged ion m/z 643.35 for spot 24 is shown. The amino acid sequence, VLQATVVAVGSGGK, was determined from mass differences in the y-fragment ion series and matched residues 40–53 of the Hsp 10. **(G)** The nanoelectrospray mass spectrum of the doubly charged ion m/z 1088.47 for spot 32 is shown. The amino acid sequence, WNTDNTLGTEITVEDQLAR, was determined from mass differences in the y-fragment ion series and matched residues 74–92 of the VDAC-1. **(H)** The nanoelectrospray mass spectrum of the doubly charged ion m/z 809.31 for spot 34 is shown. The amino acid sequence, STSETTEEAFSSSVR, was determined from mass differences in the y-fragment ion series and matched residues 180–194 of the Mitofilin. **(I)** The nanoelectrospray mass spectrum of the doubly charged ion m/z 890.85 for spot 44 is shown. The amino acid sequence, VDATEESD-LAQQYGVR, was determined from mass differences in the y-fragment ion series and matched residues 84-99 of the PDI A6 precursor. *Only y- and b-fragment ions are labeled in the spectrum.

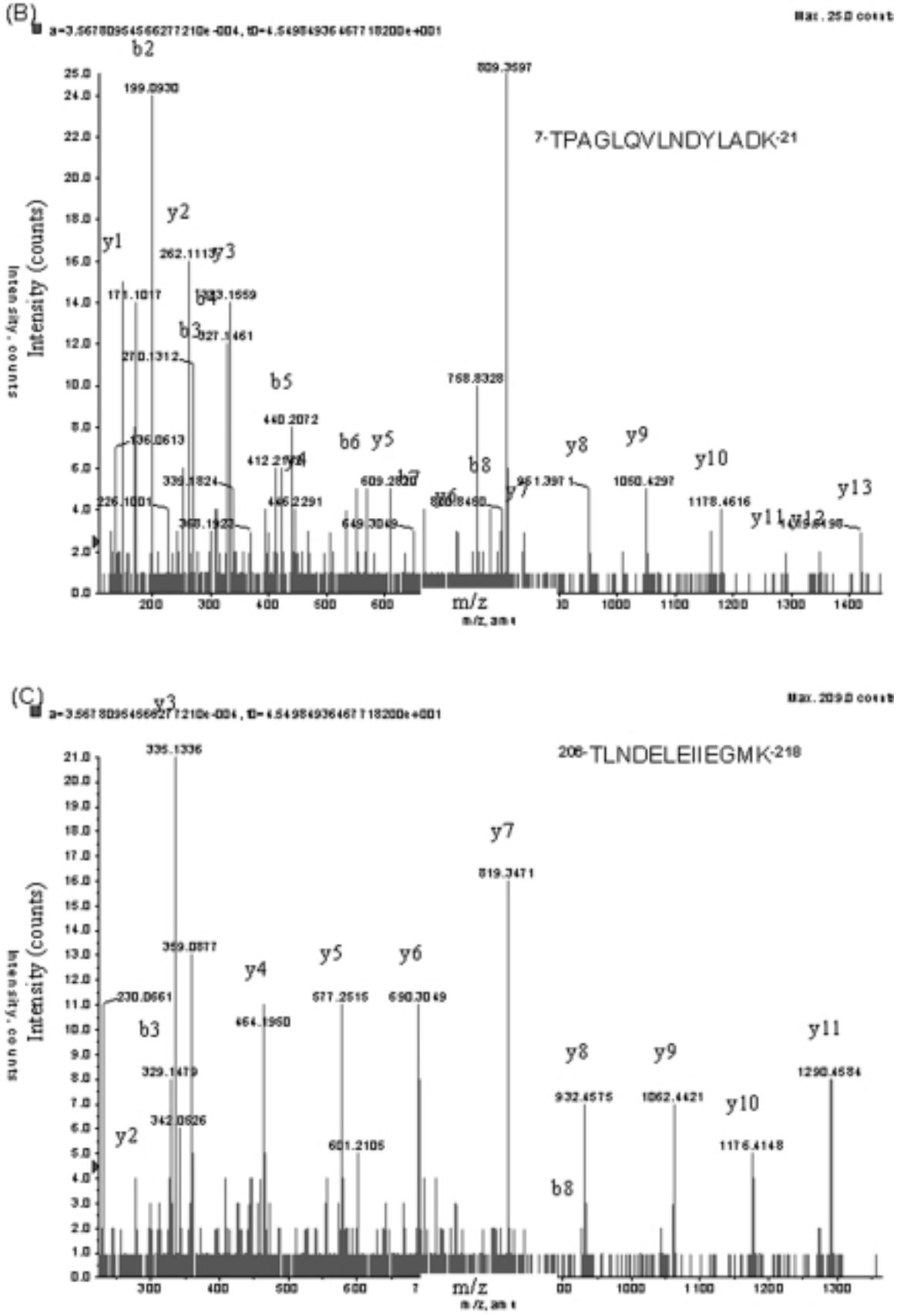

FIG. 5. (*Continued*)

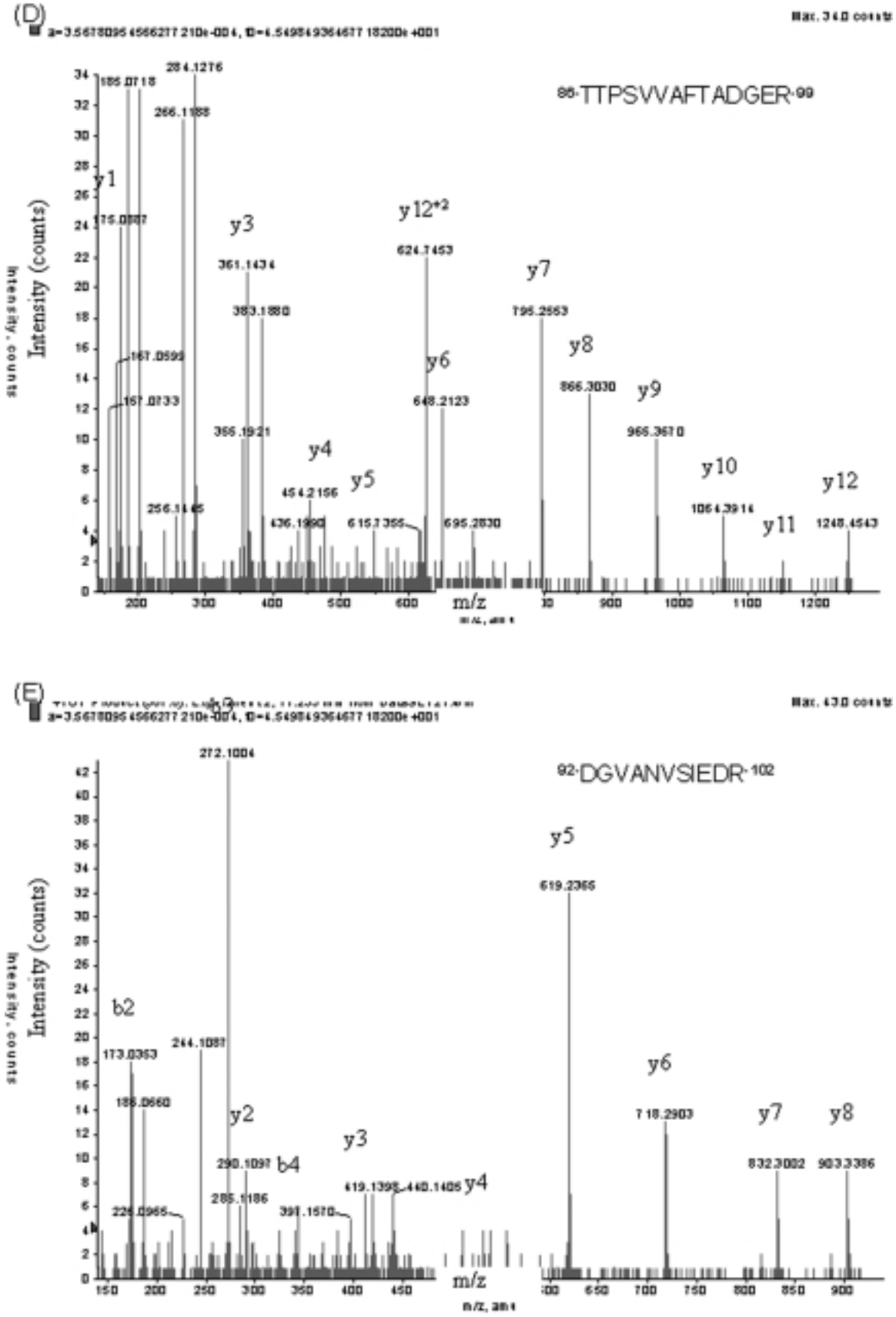

FIG. 5. (*Continued*)

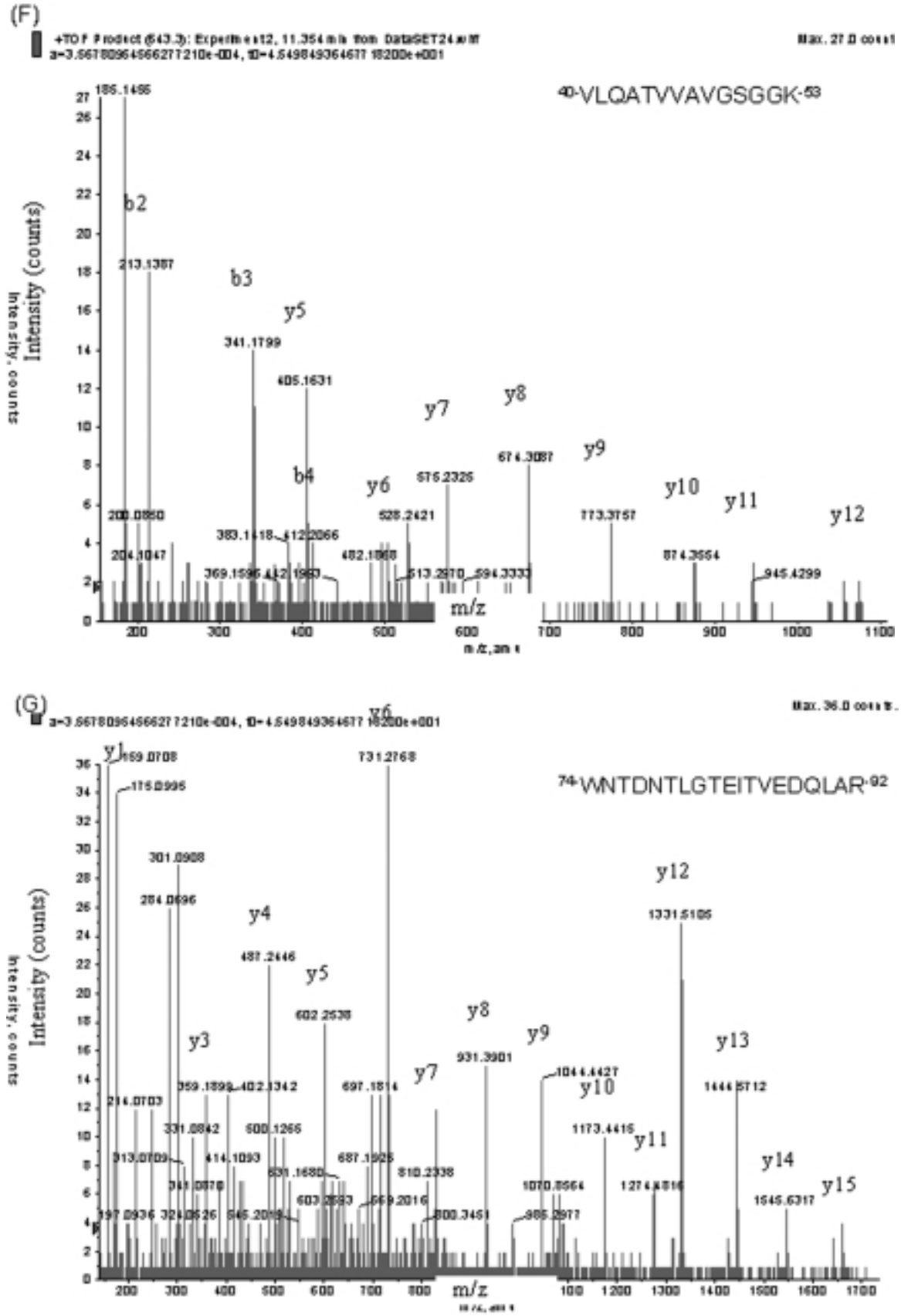

FIG. 5. (*Continued*)

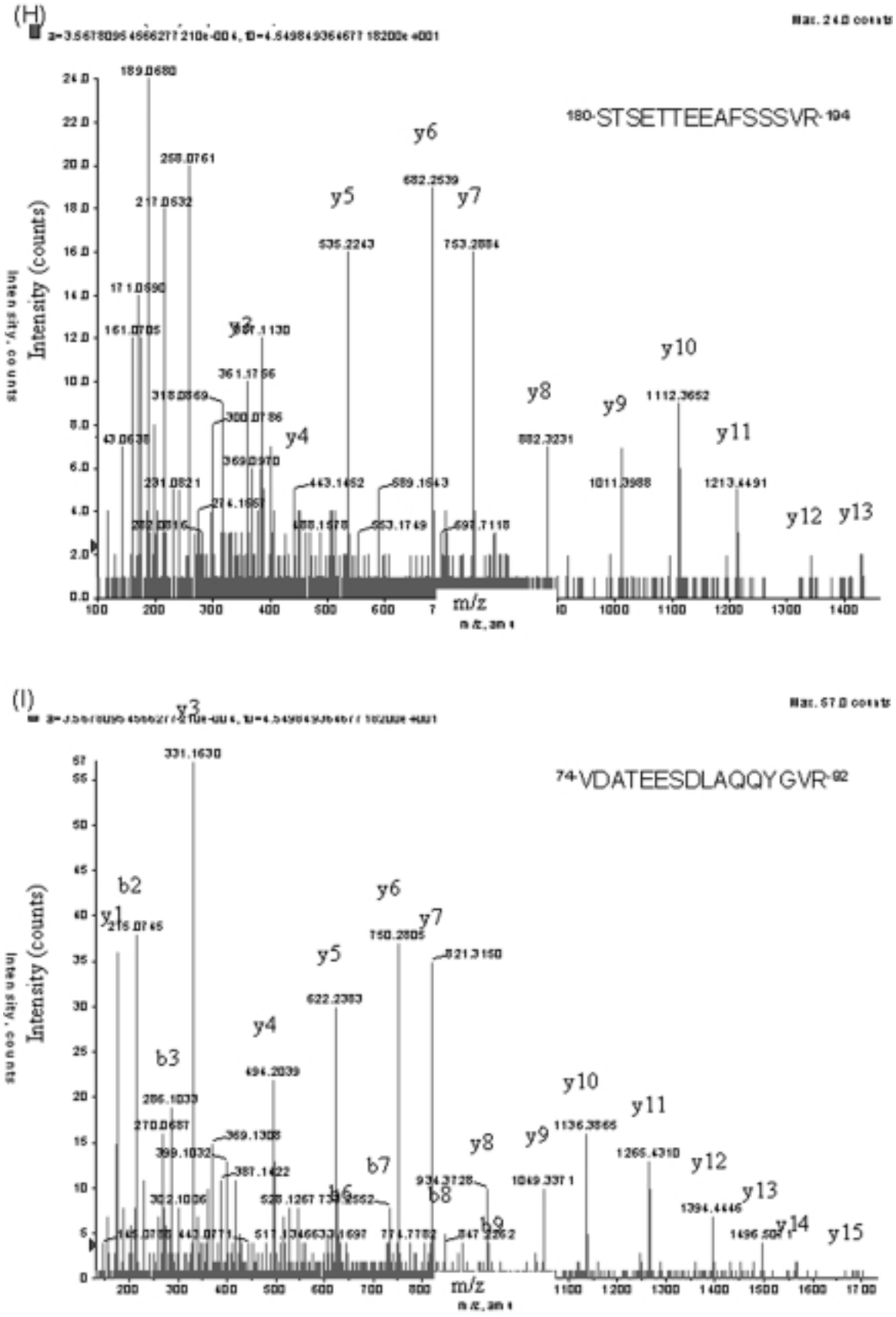

FIG. 5. (*Continued*)

The RNA expressions of the proteins

The RNA expressions of nine proteins obtained from various treatments were assayed by real-time Q-PCR (Table 3). The RNA expression in RGCs with and without the addition of aloe-emodin metabolites was compared. The results were normalized to the level of GAPDH (a housekeeping gene). The Q-PCR results revealed that the RNA levels of Cu-Zn SOD, Hsp10, and PDI A6 precursor increased in NMDA-treated RGCs, whereas those of galectin-1, EF 1-β, Hsp 60, stress-70 protein, VDAC-1, and mitofilin decreased (Table 4). Furthermore, other then the RNA levels of galectin-1 ($P = 0.025$) and mitofilin ($P = 0.02$), EF 1-β, Hsp 60, stress-70 protein, VDAC-1, and PDI A6 precursor decreased upon addition of aloe-emodin metabolites but did not reach statistical significance ($P > 0.05$; Table 4). The results were not in good agreement with the protein expressions revealed in the 2-DE gel. Several post-translational modifications, including phosphorylation, glycosylation, and degradation, which are aberrantly regulated in many diseases, may also have interfered with the results of this study, as the changes of the proteins in this study could not be predicted by measuring the amount of mRNA or by studying nucleoside sequences. Therefore, post-translational modifications of these proteins were also analyzed by nano-LC-MS/MS. Some post-translational modifications were identified in Hsp 60, stress-70 protein, VDAC-1, and the PDI A6 precursor. Hsp 60 was oxidized at M55, M256, and M177; stress-70 protein was deamidized at N268; VDAC-1 was deamidized at N61; and the PDI A6 precursor was oxidized at M326, M358, and M427 (Fig. 5A–I). The phenomena of post-translational modifications might have influenced the function of the proteins resulting in the nonparallel expressions of proteins and RNA. On the other hand, the RNA expressions of Cu-Zn SOD, Hsp 10, and PDI A6 were upregulated by aloe-emodin metabolites, which was consistent with the protein levels of the proteins obtained by the 2DE gel. Nevertheless, only the range of the increase of Cu-Zn SOD had a significant difference ($P = 0.01$; Table 4) in the expressions of RNA, whereas the increased expression of Hsp 10 and PDI A6 after adding aloe-emodin metabolites were not significantly different ($P > 0.05$; Table 4). The expression of the three proteins was also detected by Western blot and revealed correlated results (Fig. 6A and 6B) In Table 4, the results of Q-PCR revealed that there were significant differences in galectin-1, Cu-Zn SOD, and mitofilin. Nevertheless, only the RNA level of Cu-Zn SOD was increasing, which was consistent with the data of proteomics.

DISCUSSION

Proteomics has been successfully used to compare changes in protein levels that happen in a wide range of diseases.[37,38] In this study, we applied this technique to detect the mechanisms by which aloe-emodin metabolites acted as the neuroprotector in NMDA-treated N18 RGCs. By comparing the differences in protein-profile patterns between treatments with and without aloe-

Table 4. The Results of Quantitative Polymerase Chain Reaction

Treatment	*NMDA*	*NMDA + aloe-emodin s/g*	*Difference*	P-*value*
Galectin-1	1.21 ± 0.07	0.93 ± 0.12	−	0.025*
EF 1-β	0.89 ± 0.11	0.78 ± 0.09	−	0.25
Hsp60	0.80 ± 0.03	0.75 ± 0.08	−	0.37
Stress-70 protein	0.92 ± 0.10	0.85 ± 0.08	−	0.42
Cu-Zn SOD	0.71 ± 0.08	1.15 ± 0.05	+	0.01*
Hsp 10	0.64 ± 0.03	0.65 ± 0.06	+	0.48
VDAC-1	0.83 ± 0.04	0.79 ± 0.09	−	0.52
Mitofilin	1.35 ± 0.05	0.93 ± 0.09	−	0.02*
PDI A6 precursor	0.72 ± 0.03	0.75 ± 0.08	+	0.46

NMDA, *N*-methyl-d-aspartate; EF-1β, elongation factor 1-beta; Hsp, 60 kDa heat shock protein; Cu-Zn SOD, superoxide dismutase; Hsp 10, 10 kDa heat shock protein; VDAC-1, voltage-dependent anion-selective channel protein mitofilin, mitochondrial inner-membrane protein; PDI A6 precursor, protein disulfide-isomerase.

[a]The results of NMDA-treated N18 RGCs.

[b]The results of NMDA + aloe-emodin s/g treated N18 RGCs.

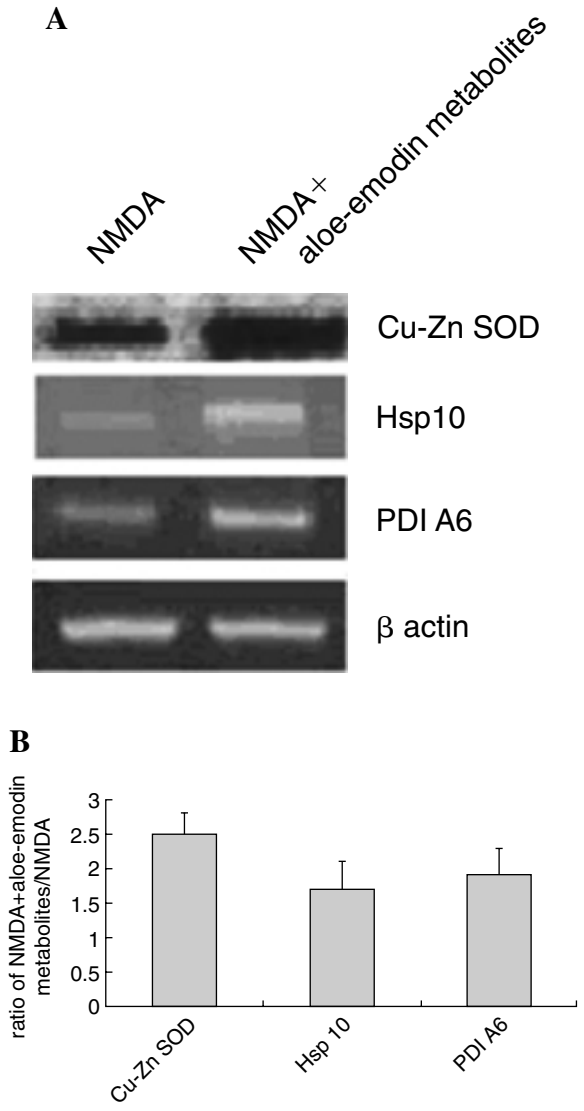

FIG. 6. (**A** and **B**) Western blotting expressions of Cu-Zn SOD, Hsp10, and PDI A6 were upregulated after aloe-emodin metabolites were added to *N*-methyl-D-aspartate treated retinal ganglion cells.

emodin metabolites in NMDA-treated N18 RGCs, we detected that some proteins were expressed in differing amounts. The results indicated that proteins involved in the regulation of energy in cells were the most prominent group to be affected by aloe-emodin metabolites and occupied 31.3%. Other proteins affected by aloe-emodin metabolites included those involved in cells' growth, formation of cells' structures, and stress-induced proteins, which regulate intracellular function. These proteins might have exerted protective effects to decrease the apoptosis of NMDA-treated N18 RGCs. Of the detected proteins, galectin-1, EF 1-β, Hsp 60, stress-70 protein, Cu-Zn SOD, Hsp 10, and VDAC-1 were prominently expressed only when aloe-emodin metabolites were added and were absent in the control group, indicating that they were induced by aloe-emodin metabolites and associated with neuroprotection. The physiologic function of galectin-1 is as an autocrine negative growth factor that regulates cell proliferation (Table 3).[39] From the data generated by Q-PCR (Table 4), galectin-1 was downregulated upon the addition of aloe-emodin metabolites. The results from Q-PCR, but not the results from proteomics, conformed to the physiologic function of galectin-1, which, as mentioned above, is a negative growth factor. The expressions of RNA and protein in galectin-1 were not equal. Nevertheless, there was no post-translation modification detected, and the diverse expression of RNA and protein in galectin-1 may owing to other influences, such as protein-protein interaction. EF-1 was reported to stimulate the exchange of GDP bound to EF-1-alpha to GTP and to affect the GDP/GTP exchange,[40] which is closely related to the activity and lifespan of cells. The functions of Hsp 60, stress-70 protein, and Hsp 10 have been reported to be involved in mitochondrial protein import, control of cell proliferation, cellular aging, and to possibly act as a chaperone.[41] Hsp 60, stress-70 protein, and Hsp 10 were often upregulated when conflicted with stress. In this study, the results of Q-PCR revealed that the RNA of EF-1-alpha, Hsp 60, and stress-70 were downregulated in the aloe-emodin metabolites added to RGCs; this result was not identical to the expressions in the 2-DE gel and did not conform to their physiologic functions. The discrepancy in the expression of Hsp 60 and stress-70 might have resulted from the post-translational modifications of these proteins, because Hsp 60 was oxidized at M55, M256, and M177, and stress-70 protein was deamidized at N268. Post-translational modification of proteins may affect the function of proteins and change the fate of cells, and this may explain the different expression of these proteins from the results of proteomics and Q-PCR. Regarding EF-1-alpha, there were no post-translational modifications detected; determining the exact role of EF-1-alpha will require further investigation. Hsp 10 was upregulated upon the addition of aloe-emodin, this result was identical to its expression in the 2-

DE gel and conformed to its physiologic function. Nevertheless, there was no significant difference in the expression of RNA levels of Hsp 10. Cu-Zn SOD has been shown to destroy free radicals and to be an important molecule in antioxidation.[42] The results of Q-PCR revealed that the RNA level of Cu-Zn SOD was upregulated by the addition of the aloe-emodin metabolites and showed a statistical difference; this was consistent with its expression in the 2-DE gel and its physiologic function. The expression of Cu-Zn SOD was the most affirmable of all the proteins analyzed in this study. The RNA level of VDAC-1 was downregulated by NMDA and further down-regulated by the addition of aloe-emodin metabolites. VDAC-1 has been reported to form a channel through the mitochondrial outer membrane, as well as the plasma membrane.[43] Besides, mitofilin is a mitochondrial inner membrane protein[44]; it plays an important role in the apoptosis process and in the changing of mitochondrial membrane potential. The expressions of the protein levels of VDAC-1 and mitofilin were not identical to that of 2-DE gel. Although there are diverse functions of VDAC-1 and mitofilin, the expressions of the proteins could not be predicted. There was no reasonable explanation for the expressions of RNA and protein levels of VDAC-1 and mitofilin in this study and would require a more advanced investigation. The PDI A6 precursor functions in the rearrangement of S-S bonds in proteins.[45] The RNA level of the PDI A6 precursor was upregulated by the addition of aloe-emodin metabolites, which was consistent with the result of 2-DE. Nevertheless, the results did not have a statistical difference. Several post-translational modifications of the PDI A6 precursor at M326, M358, and M427 with oxidation were detected, but the oxidative modification often did not interfere with its protein expression. The reasonable explanation for the diverse expressions of the levels of RNA and protein of PDI A6 also would require a more advanced investigation.

We had identified some proteins involved in the neuroprotection effects of the aloe-emodin metabolites. These proteins were associated with the regulation of energy, apoptosis, and oxidation in cells. In conclusion, the effects of aloe-emodin metabolites on the NMDA-treated RGCs were closely associated with the regulation of apoptosis and antioxidation. Nevertheless, the results of RNA levels were not completely consistent with those of the 2-DE gel. We hypothesized that this may owing to the occurrence of instability of mRNA, protein-protein interaction during translation, or post-translation modifications. Besides, the global condition was not the same before and after NMDA and aloe-emodin metabolites were added and might have influenced the expression of the protein. It is important to take the protein expression and RNA levels together in order to view the mechanism and pathways of the reaction in the study. Among the studied molecules, RNA and protein expressions of Cu-Zn SOD, Hsp 10, and PDI A6 were identical. In the three proteins, only the RNA level of Cu-Zn SOD had a significant difference after aloe-emodin metabolites was added (Table 4), and this result was also proved by Western blotting (Fig. 6A and 6B). Cu-Zn SOD may be a very important molecule in the pathway of aloe-emodin metabolites in reducing apoptosis in NMDA-treated N18 RGCs. We supposed that 15 μM of aloe-emodin metabolites, by way of scavenging the free-radical effect of Cu-Zn SOD, protected NMDA-treated N18 RGCs. The exact effects of Cu-Zn SOD may require a more advanced investigation to understand its complete role. But this did not mean that other proteins detected by the 2-DE gel and nano-LC-MS/MS analyses were not important. These proteins might also be involved in the mechanisms of the reaction of aloe-emodin metabolites, but they require further studies to prove their effects. Besides, glutamate cytotoxicity may not be the issue of an acute rise in IOP.[46] Consequently, we will test the effects of aloe-emodin metabolites and proteins involved in different stresses induced by apoptosis in N18 RGCs in the future. Under pathologic conditions, chronic low-grade overactivation of the NMDA receptor causes an excessive amount of Ca^{+2} influx into the nerve cell, which then triggers a variety of processes that can lead to apoptosis. Overloading of Ca^{+2} will result in the formation of the oxygen free radical. Overloading of Ca^{+2} activates neuronal nitric oxide synthase (NOS) increases the production of nitric oxide (NO) and the formation of toxic peroxynitrite ($ONOO^{-}$). These changes activate transcription factors that can penetrate the nucleus and influence neuronal injury and apoptosis. Consequently, NMDA-induced apoptosis in RGCs could be suppressed by aloe-emodin through the regulation of the antioxidant, Cu-Zn SOD.

CONCLUSIONS

Aloe-emodin metabolites are a potential agent for the neuroprotective therapy of glaucomatous patients by destroying free radicals to reduce apoptosis in RGCs.

REFERENCES

1. Wolfs, R.C., Borger, P.H., Ramrattan, R.S., et al. Changing views on open-angle glaucoma: Definitions and prevalences. *Invest. Ophthalmol. Vis. Sci.* 41: 3309–3321, 2000.
2. Klemett, A. Low-tension glaucoma—a disease for ophthalmology or internal medicine? *Duodecim.* 113:1425–1426, 1997.
3. Koss, M.C. Functional role of nitric oxide in regulation of ocular blood flow. *Eur. J. Pharmacol.* 374:161–174, 1999.
4. Garcia-Valenzuela, E., Shareef, S., Walsh, J., et al. Programmed cell death of retinal ganglion cells during experimental glaucoma. *Exp. Eye Res.* 61:33–44, 1995.
5. Dreyer, E.B., and Grosskreutz, C.L. Excitatory mechanisms in retinal ganglion cell death in primary open angle glaucoma (POAG). *Clin. Neurosci.* 4:270–273, 1997.
6. Hauben, E., Nevo, U., Yoles, E., et al. Autoimmune T-cells as potential neuroprotective therapy for spinal cord injury. *Lancet* 355:286–287, 2000.
7. Moalem, G., Leibowitz-Amit, R., Yoles, E., et al. Autoimmune T-cells protect neurons from secondary degeneration after central nervous system axotomy. *Nat. Med.* 5:49–55, 1999.
8. Schori, H., Yoles, E., and Schwartz, M. T-cell-based immunity counteracts the potential toxicity of glutamate in the central nervous system. *J. Neuroimmunol.* 119:199–204, 2001.
9. Schwartz, M., and Kipnis, J.G. Genetic control of immune response to trauma: Vaccination for acute and chronic CNS degenerative disorders. *Trends Mol. Med.* 7:252–258, 2001.
10. Bakalash, S., Kessler, A., Mizrahi, T., et al. Antigenic specificity of immunoprotective therapeutic vaccination for glaucoma. *Invest. Ophthalmol. Vis. Sci.* 44: 33374–33381, 2003.
11. Lipton, S.A., and Rosenberg, R.A. Mechanisms of disease: Excitatory amino acids as a final common pathway in neurologic disorders. *N. Engl. J. Med.* 330: 613–622, 1994.
12. Kaul, M., Garden, G.A., and Lipton, S.A. Pathways to neuronal injury and apoptosis in HIV-associated dementia. *Nature* 410:988–994, 2001.
13. Nucci, C., Tartaglione, R., Rombola, L., et al. Neurochemical evidence to implicate elevated glutamate in the mechanisms of high intraocular pressure (IOP)-induced retinal ganglion cell death in rat. *Neurotoxicology* 26:935–941, 2005.
14. Luo, X., Heidinger, V., Picaud, S., et al. Selective excitotoxic degeneration of adult pig retinal ganglion cells in vitro. *Invest. Ophthalmol. Vis. Sci.* 42:1096–1106, 2001.
15. Kido, N., Tanihara, H., Honjo, M., et al. Neuroprotective effects of brain-derived neurotrophic factor in eyes with NMDA-induced neuronal death. *Brain Res.* 884:59–67, 2000.
16. Dreyer, E.B., Zurakowski, D., Schumer, R.A., et al. Elevated glutamate levels in the vitreous body of humans and monkeys with glaucoma. *Arch. Ophthalmol.* 114:299–305, 1996.
17. Brooks, D.E., Garcia, G.A., Dreyer, E.B., et al. Vitreous body glutamate concentration in dogs with glaucoma. *Am. J. Vet. Res.* 58:864–867, 1997.
18. Sucher, N.J., Aizenman, E., and Lipton, S.A. *N*-methyl-D-aspartate antagonists prevent kainate neurotoxicity in rat retinal ganglion cells *in vitro*. *J. Neurosci.* 11:966–971, 1991.
19. Zeevalk, G.D., and Nicklas, W.J. Evidence that the loss of the voltage-dependent Mg^{2+} block of the *N*-methyl-D-aspartate receptor underlies receptor activation during inhibition of neuronal metabolism. *J. Neurochem.* 59:1211–1120, 1992.
20. Yoles, E., and Schwartz, M. Elevation of intraocular glutamate levels in rats with partial lesion of the optic nerve. *Arch. Ophthalmol.* 116:906–910, 1998.
21. Yoles, E., and Schwartz, M. Degeneration of spared axons following partial white matter lesion: Implications for optic nerve neuropathies. *Exp. Neurol.* 153:1–7, 1998.
22. Neacsu, A., Oprean, C., Curea, M., et al. Neuroprotection with carotenoids in glaucoma. *Oftalmologia* 59:70–75, 2003.
23. Ferreira, S.M., Lerner, S.F., Brunzini, R., et al. Oxidative stress markers in aqueous humor of glaucoma patients. *Am. J. Ophthalmol.* 137:62–69, 2004.
24. Kang, J.H., Pasquale, L.R., Willett, W., et al. Antioxidant intake and primary open-angle glaucoma: A prospective study. *Am. J. Epidemiol.* 158:337–346, 2003.
25. Gu, J.W., Hasuo, H., Takeya, M., et al. Effects of emodin on synaptic transmission in rat hippocampal CA1 pyramidal neurons *in vitro*. *Neuropharmacology* 49:103–111, 2005.
26. Mijatovic, S., Maksimovic-Ivanic, D., Radovic, J., et al. Aloe-emodin prevents cytokine-induced tumor cell death: The inhibition of autotoxic nitric oxide release as a potential mechanism. *Cell Mol. Life Sci.* 6:1805–1815, 2004.
27. Lee, H.Z., Wu, C.H., and Chang, S.P. Release of nucleophosmin from the nucleus: Involvement in aloe-emodin-induced human lung non-small-carcinoma cell apoptosis. *Int. J. Cancer* 113:971–976, 2005.
28. Lee, H.Z., Hsu, S.L., Liu, M.C., et al. Effects and mechanisms of aloe-emodin on cell death in human lung squamous-cell carcinoma. *Eur. J. Pharmacol.* 431:287–295, 2001.
29. Olthof, M.R., Hollman, P.C., Vree, T.B., et al. Bioavailabilities of quercetin-3-glucoside and quercetin-4′-

glucoside do not differ in human. *J. Nutr.* 130:1200–1203, 2000.
30. Hsiu, S.L., Huang, T.Y., Hou, Y.C., et al. Comparison of metabolic pharmacokinetics of naringin and naringenin in rabbits. *Life Sci.* 70:1481–1489, 2002.
31. Fang, S.H., Hou, Y.C., Chang, W.C., et al. Morin sulfates/glucuronides exert anti-inflammatory activity on activated macrophages and decreased the incidence of septic shock. *Life Sci.* 74:743–756, 2003.
32. Futcher, B., Latter, G.I., Monardo, P., et al. A sampling of the yeast proteome. *Mol. Cell Biol.* 19:7357–7368, 1999.
33. Griffin, T.J., Gygi, S.P., Ideker, T., et al. Complementary profiling of gene expression at the transcriptome and proteome levels in *Saccharomyces cerevisiae*. *Mol. Cell Prot.* 1:323–333, 2002.
34. Terry, D.E., Umstot, E., and Desiderio, D.M. Optimized sample-processing time and peptide recovery for the mass spectrometric analysis of protein digests. *J. Am. Soc. Mass Spect.* 15:784–794, 2004.
AU11 35. Hirosawa, M., Hoshida, M., Ishikawa, M., et al. *Comput. Appl. Biosci.* 9:161–167, 1993.
36. Livak, K.J., and Schmittgen, T.D. Analysis of relative gene expression data using real-time quantitative PCR and the 2(-Delta Delta C(T)) Method. *Methods* 25:402–408, 2001.
AU12 37. Glimann, C., Sheehan, K., Kay, E., et al. *J. Pathol.* 208:595–606, 2006.
38. Witt, A.E., Hines, L.M., Collins, N.L., et al. Functional proteomics approach to investigate the biological activities of cDNAs implicated in breast cancer. *J. Prot. Res.* 5:599–610, 2006.
AU13 39. Lovegrove, C. Galectin-1: A novel hypoxia-induced protein linked with tumor immune privilege. *Nat. Clin. Pract. Oncol.* 3:6, 2006.
AU13 40. Tomlinson, V.A., Newbery, H.J., Wray, N.R., et al. Translation elongation factor eEF1A2 is a potential oncoprotein that is overexpressed in two-thirds of breast tumours. *BMC Cancer* 5:113, 2005.
41. Rylander, M.N., Feng, Y., Bass, J., et al. Thermally induced injury and heat-shock protein expression in cells and tissues. *Ann. N.Y. Acad. Sci.* 1066:222–242, 2006.
42. Zhang, H.W., Wang, F.S., Shao, W., et al. Characterization and stability investigation of cu,zn-superoxide dismutase covalently modified by low-molecular-weight heparin. *Biochemistry (Moscow)*. 71(Suppl. 1):S96–S100, 2006.
43. Okada, S.F., O'Neal, W.K., Huang, P., et al. Voltage-dependent anion channel-1 (VDAC-1) contributes to ATP release and cell-volume regulation in murine cells. *J. Gen. Physiol.* 124:513–526, 2004.
44. Myung, J.K., Gulesserian, T., Fountoulakis, M., et al. Deranged hypothetical proteins Rik protein, Nit protein 2, and mitochondrial inner membrane protein, mitofilin, in fetal Down syndrome brain. *Cell Mol. Biol. (Noisy-le-grand).* 49:739–746, 2003.
45. Ciaffi, M., Paolacci, A.R., D'Aloisio, E., et al. Cloning and characterization of wheat PDI (protein disulfide isomerase) homoeologous genes and promoter sequences. *Gene* 366(1):209–218, 2006.
46. Ben Simon, G., Bakalash, J., Aloni, E.S., et al. A rat model for acute rise in intraocular pressure: Immune modulation as a therapeutic strategy. *Am. J. Ophthalmol.* 141:1105–1111, 2006.

Reprint Requests: *Fuu-Jen Tsai*
Department of Medical Genetics and Pediatrics
China Medical University Hospital
No. 2 Yuh-Der Road
Taichung 404, Taiwan

E-mail: d0704@www.cmuh.org.tw

LIN

AU1
City?

AU2
Spell out “pI”.

AU3
City and state?

AU4
City and state?

AU5
Name, city, and state of manufacturer?

AU6
City and state?

AU7
City and state?

AU8
Supply missing characters.

AU9
Spell out “MWs”.

AU10
Please confirm page range in Ref. 10.

AU11
Provide name of article in Ref. 35.

AU12
Provide name of article in Ref. 37.

AU13
Provide full page range in Refs. 39 and 40.